https://doi.org/10.1016/j.eurpolymj.2020.109884

Influence of silica aerogel particles on the foaming process and cellular structure of rigid polyurethane foams

Paula Cimavilla-Román[a]*, Saul Pérez-Tamarit[a], Mercedes Santiago-Calvo[a], Miguel Ángel Rodríguez-Pérez[a]

[a] Cellular Materials Laboratory (CellMat), Condensed Matter Physics Department, University of Valladolid, Paseo Belen 7, Valladolid 47011, Spain

* Correspondence: Paula Cimavilla Román (E-mail: paulacimavilla@fmc.uva.es)

Abstract

Water blown rigid polyurethane (RPU) composite foams were produced using different concentrations of nanoporous silica aerogel micrometric powder (0.5, 1 and 3 wt%). The effect of these particles on the foaming kinetics was analysed from a physical and chemical viewpoint. On the physical side, the foaming process was studied by *in-situ* X-ray radioscopy. The inclusion of aerogel particles in the system delays the foam expansion and enhances the nucleation of cells. However, high amounts of these particles (3 wt%) lead to intense cell coalesce during foam evolution. On the chemical side, the reaction kinetics was investigated by *in-situ* FTIR spectroscopy and reaction temperature measurements. The addition of low contents of aerogel (below 3 wt%) reduces the conversion of isocyanate while favouring the generation of urethane groups, which explains the higher density of the foams with low aerogel contents. However, the foam with high contents of aerogel (3 wt%) does not change the reaction balance in comparison to the reference. Therefore, this foam presents similar expansion and density to those of Reference. Furthermore, higher reaction temperatures were reached by the reference foam during the foaming process, and higher dissipation speeds of these temperatures were detected for the foams containing aerogel with respect to those of the reference foam.

Keywords

Polyurethane foam; Composite foams; Nanoporous silica aerogel; X-ray radioscopy; Reaction kinetics; FTIR spectroscopy; *In-situ* studies

1 Introduction

Polymer composite foams are very promising materials due to the enhanced properties that result from the synergy of the polymer and filler particle attributes. Micro and nanosized fillers reinforce the polymer matrix and modify the final cellular structure. These synergistic effects can result in materials with increasing strength [1,2], fire resistance [3] and thermal insulation capabilities [4–6]. In addition, the inclusion of fillers permits tailoring the cellular structure. For all these reasons, these materials have significant potential in the automotive, construction and electronic industries [7].

One of the most interesting thermoset polymeric foams is rigid polyurethane (RPU) foam, widely employed in the construction industry. RPU foams are one of the most popular thermal insulation materials for their low thermal conductivity (16–35 mW/(m·K)) and low density (25–50 kg/m^3) [8]. These materials are produced as a result of two main exothermic reactions: polymerization reaction between isocyanate and polyol; and blowing reaction between isocyanate and water. The polymerization reaction is responsible for the generation of urethane linkages and the consequent polymerization process [8]. Meanwhile, the blowing reaction forms urea hard segments and promotes the production of CO_2 gas resulting in the foam rise. The presence of fillers has been reported to introduce significant modifications not only on the final foam properties but also on the physical mechanisms that are responsible for the foam formation [9,10] and the chemical balance between RPU reactions [5,10,11]. Among other effects, the use of fillers has been proven to permit the production of foams with more homogeneous cellular structures, smaller cells and lower densities, becoming materials particularly suitable for thermal insulation purposes [4,12,13]. Due to these cellular structure improvements, many types of fillers have been tested to improve the applicability and performance of RPU foams, such as nanoclays [4,14], nanosilicas [15], graphite [16] and different carbon fillers [11,13,17]. In addition, over the last few years, the use of advanced and multi-functional materials, like super-insulating silica aerogel, as fillers for composite materials, has started to attract increasing attention [5,18–21]. Nanoporous silica aerogels presents exceptional properties that make them very suitable thermal insulators and a very attractive additive to reduce the thermal conductivity of RPU foams. Some of the key properties of these materials are a low thermal conductivity between (10–30 mW/m·K), a low density (0.003-0.35 g/cm^3), a high porosity (~85%-99.87%) and a high specific surface area (~600-1000 m^2/g) [22,23]. However, some characteristics of these aerogels like its highly open structure, low connections between secondary particles, low density and high porosity make this

material brittle which dramatically limits their exploitation as insulation materials by themselves [24].

Despite the interesting properties of this material, the use of silica aerogel as an additive of polymeric materials has just started to be exploited. Most research works that can be found in the literature are focused on studying the effect of aerogel on the thermal conductivity of RPU foams [18–20]. Zhao et al. [18] prepared Polyisocyanurate rigid (PIR) foams containing 1 wt%, 2 wt%, 3 wt%, 4 wt%, 5 wt%, 6 wt% and 8 wt% of granular silica aerogel. The foam with 8 wt% of aerogel showed a reduction of the thermal conductivity by 34.6%. The oxygen index of the same foam was also measured, revealing an improvement in flame retardant properties. Although the cellular structure was not characterised in depth, SEM images showed how the incorporation of aerogel alters the homogeneity of the PIR foams cellular structure. Nazeran and Moghaddas [20] produced cyclopentane blown RPU foams reinforced with different contents of non-commercial nanometric silica aerogel (1 wt%, 3 wt%, and 5 wt%). The composite foams were produced following two different routes, one adding silica aerogel to MDI raw material and second to the polyol phase. In both cases, the authors observed more homogeneous cellular structures and a reduction in the cell size when adding aerogel particles up to a 3 wt%. However, increasing the aerogel content up to the 5 wt% increased the mean cell size due to the viscosity increase of the polyol and the isocyanate. Comparison of the cellular structures produced by the two production routes revealed that the addition of aerogel to the MDI matrix results in materials with smaller cells and narrower cell size distribution, probably due to the low viscosity of MDI relative to the polyol. Concerning the thermal insulation capabilities, by increasing the silica aerogel content from 0 wt% to 5 wt%, the thermal conductivity was reduced by 14.6%. Dourbash et al. [19] prepared silica aerogel rigid polyurethane composite foams. Contents of 3 wt% and 4 wt% of both granular (with particle size from 0.7 to 4 mm) and powdered (particle size from 0.05 to 1 mm) silica aerogel particles were used to prepare the foams. The resulting composite foams did not show a reduction in the thermal conductivity, which was explained considering the deterioration of the cellular structure, and the increase in the average cell size. As mentioned previously, these research works are mainly focused on the properties of the RPU foams containing aerogel particles, but they did not analyse the foaming process and in particular the influence on the aerogel particles on the physical and chemical mechanisms taking place during the production of the RPU foams. Therefore, there is still a lack of knowledge about how aerogel particles affect the reactive foaming process and the final cellular structure.

Hence, this work aims at evaluating the influence of powdered silica aerogel on the physicochemical mechanisms leading to the formation of water blown RPU foams.

To this end, different *in-situ* techniques have been used due to the impossibility of stopping the chemical reactions responsible for the generation of RPU foams. On the one hand, the foaming process has been studied from a physical perspective using X-ray radioscopy. This technique enables to monitor the evolution of the main features of RPU foams while foaming, such as relative density, cell size and cell nucleation density [9,25] and allows to analyse nucleation, growing and degeneration mechanisms. On the chemical side, the kinetics of the two main reactions of the RPU foam formation have also been followed. The generation of urethane and urea products has been monitored by means of *in-situ* FTIR spectroscopy. Furthermore, thanks to the exothermic nature of these reactions it has been possible to obtain the internal temperature evolution while foaming by suitably positioning thermocouples inside the foaming mould [5] providing information about the global reaction kinetics of the materials under analysis.

The knowledge gained by this research will be useful to optimise RPU formulations containing silica aerogels in order to take full advantage of the excellent properties of this nanoporous material to reduce the thermal conductivity of RPU foams.

2 Materials and methods

2.1 Materials

2.1.1 Reactants of RPU foams

The polyol component used was a blend of two high functionality polyether polyols, Alcupol R4520 (functionality of 4.5, OH value of 455 mg·KOH/g) and Alcupol R3810 cross-linker (functionality of 3, OH value of 380 mg·KOH/g), both from Repsol S.A. The isocyanate was a polymeric diphenylmethane diisocyanate (pMDI), IsoPMDI 92140 (31.5% NCO, density 1.23 g cm^{-3}, viscosity 170-250 mPas) supplied by BASF. TEGOAMIN® DMCHA (N,N-dimethylcyclohexylamine) from Evonik was employed as a catalyst, that is a tertiary amine used primarily to promote the urethane (polyol-isocyanate) reaction. TEGOSTAB® B8522 (a non-hydrolysable polyether-polydimethyl-siloxane–stabilizer) from Evonik was used as a surfactant to obtain superior cell structures. Distilled water was employed as a blowing agent.

2.1.2 Silica aerogel fillers

Enova® Aerogel IC3100 powder, provided by Cabot, was the filler selected for the manufacturing of RPU composite foams. According to the supplier, Enova aerogels are nanoporous lightweight materials with a particle size from 2 to 40 μm, an average pore diameter of 20 nm, a particle density near 150 kg/m^3 and a very low

thermal conductivity of 12 mW/m·K. This powder is made from silica particles with a hydrophobic [(trimethylsilyl)oxy] superficial treatment [26]. This treatment replaces the hydrophilic unreacted OH groups on the surface of the aerogel skeleton (Fig. 1 a) by [(trimethylsilyl)oxy] groups that inhibit the absorption of water, resulting in hydrophobic aerogels (Fig. 1 b).

a. b.

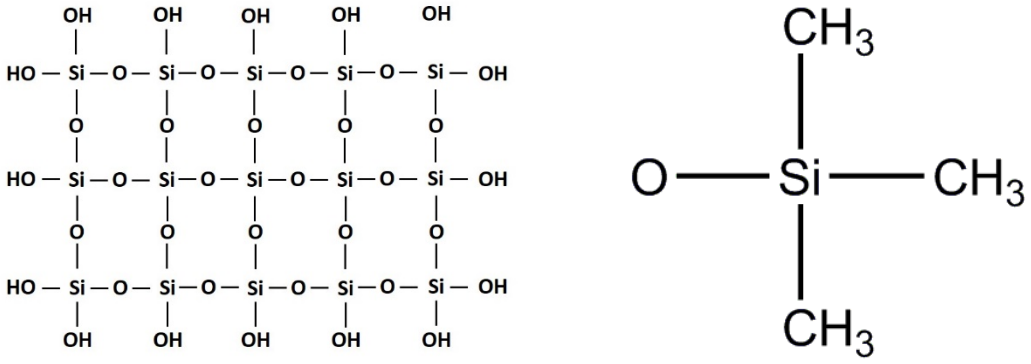

Fig. 1: a. Schematic representation of the silica aerogel particles, and b. representation of the surface modifiers groups replacing the OH groups in the left scheme.

2.2 Methods

2.2.1 Preparation of RPU composite foams

RPU foams were prepared from 90 phpp (parts per hundred parts of polyol) of Alcupol R4520, 10 phpp of Alcupol R3810, 1 phpp of TEGOSTAB B8522, 0.4 phpp of TEGOAMIN DMCHA, 4 phpp of distilled water and 197 phpp of IsoPMDI 92140. For comparison purposes, four foams with different filler content (0 wt%, 0.5 wt%, 1 wt%, 3 wt%) dispersed in the isocyanate were produced.

The blend of the polyols with the different components was performed with an overhead stirrer (EUROSTAR 60 control from IKA), equipped with a 50 mm diameter Vollrath™ Lenart-disc stirrer. First, the mixture of the polyol with the additives (catalyst, surfactant and blowing agent) was performed at 250 rpm for 2 minutes. The dispersion of the aerogel powder in the isocyanate component was carried out at low shear stress values of 250 rpm for 5 minutes. Finally, to promote the foam formation, a mixture of 50 g of isocyanate and polyol components was produced using 1200 rpm during 10 s.

A lower amount of TEGOAMIN DMCHA catalyst (0.4 ppw) is used in this study because a long cream time (around 50 seconds in our formulation) is necessary to properly observe the foaming behaviour with the X-ray setup [11,25,27]. The placement of the evolving sample inside the X-ray cabinet takes around 50 seconds, time in which monitoring with the setup used in this research is not possible.

2.2.2 Fillers characterisation

Two methods were used for the characterisation of the commercial Enova aerogel particles. Surface groups and chemical structure have been investigated employing an FTIR spectrometer model Tensor 27 (Bruker), working in the attenuated total reflectance (ATR) mode. The morphology and porous structure of the particles have been observed using high-resolution micrographs obtained by a scanning electron microscope (SEM) model QUANTA 200 FEG. Prior to the observation, the particles were dissolved in ethanol and sonicated for 30 minutes to avoid agglomerates. Then, a drop of the solution was deposited on an SEM specimen stub for the observation.

2.2.3 Density, cell size and open cell content characterisation

The produced foams were characterised using the following techniques. Foam density was measured as described by ASTM D1622/D1622M-14 [28]. Density was determined in three different samples for each material, with a diameter of 30 mm and a height of 30 mm. After measuring the densities in the samples, open cell content (OC%) was measured by using a gas pycnometer Accupyc II 1340 from Micromeritics, according to ASTM D6226-10 [29]. Relative density was obtained as the ratio between the foam density and the solid material density (1180 kg/m^3). A micro-computed tomography scan (resolution of 2.5 μm) was performed on cylindrical samples of 2.5 mm in diameter to measure the average cell size [30].

2.2.4 Time-resolved radiography (X-ray radioscopy)

The setup used for radiography acquisition (Fig. 2 a.) consists of an X-ray microfocus source from Hamamatsu with a maximum output power of 20 W (spot size: 5 μm, voltage: 20-100 kV, current: 0-200 μA). X-rays come out of the source window, forming a cone-beam of 39°, which allows to obtain up to 20 times magnification [15]. The X-ray transmitted radiation is detected by a high sensitivity flat panel connected to a frame grabber (Dalsa-Coreco) that records the radiographic images. This high-resolution detector is composed of a matrix of 2240x2344 pixels with a pixel size of 50 μm. The digital output is a 12 bits grey depth resolution, and the maximum acquisition rate goes up to 9 fps (at 4x4 pixel binning) [11].

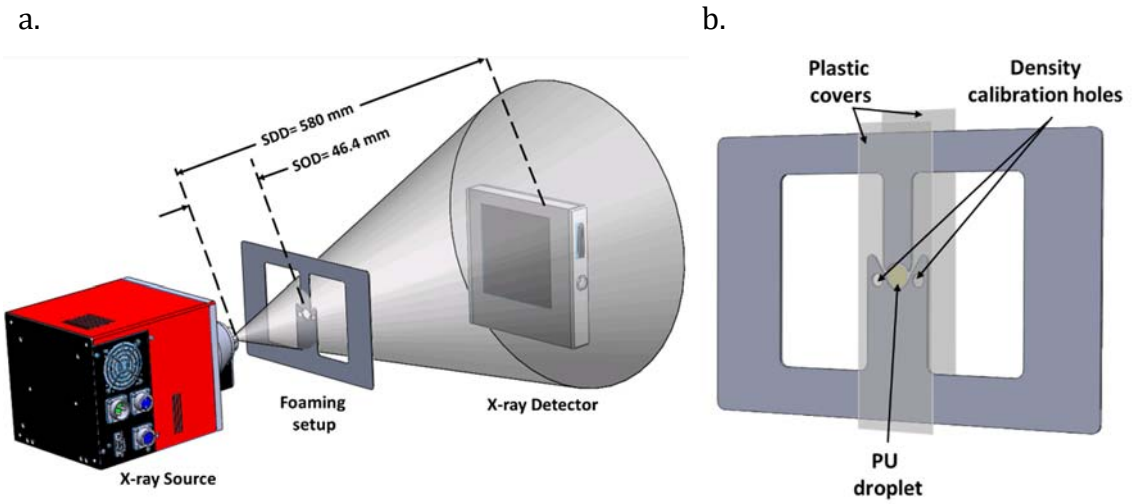

Fig. 2: X-ray setup employed for the radioscopy experiments. a. X-ray system and position of the foaming frame with respect to the X-ray source and detector and b. Stainless steel mould for PU foaming (foaming frame).

This setup is optimised for low absorbing materials such as polymers and typically works at low energies and high currents (40 kV, 120 µA) to optimise the contrast in the radiographs. To this end, the exposure time should always be set between 1-2 s. However, as the foaming process of RPU foams is swift, high acquisition rates are required to obtain images containing sharp features. For this reason, the detector was set to work under 2x2 binning mode [31] with an acquisition time of 800 ms (1.25 fps) (thus effective exposure time of 3.2 s). Consequently, the effective pixel size (after applying 2x2 binning) is increased from 3.85 µm to 7.70 µm.

In these experiments, a 0.6 mm-thick stainless-steel frame was employed (Fig. 2 b.) to produce the foams. This frame has a circular cavity (Ø =6 mm) where a PU reacting droplet of approximately 0.02 mL is placed. The droplet is taken from the cup where the 50 g polyol-isocyanate mixture is performed (section 2.2.1). Two evacuating conducts facilitate the foam evacuation out of the central circular cavity improving the X-ray imaging in the central region of the cavity; therefore, cell growth can be visualised and further analysed. In order to avoid the PU drop from flowing and growing in the thickness direction, two polypropylene covers (thickness~50 µm) were employed. This ensured having a quasi-bidimensional foam system with a constant thickness in which only a few cells are present in the thickness direction. Besides, two circular holes (Fig. 2 b.) located in the frame hold two reference materials, air (density 1 kg/m^3, porosity 1) and a thermoplastic polyurethane (TPU) pellet of thickness 0.6 mm (density 1106.9 kg/m^3, porosity 0), which are used for relative density calibration purposes.

Once the radiography sequence has been acquired, it is necessary to treat the images to obtain numerical results. The evolution of three different foam descriptors were measured: density, cell size, and cell nucleation density.

The density can be calculated from each radiograph, thanks to Beer-Lambert law [32] (Eq. 1). This expression predicts the attenuation of an incident monochromatic X-ray beam (I_{air}) by an exponential function of the linear absorption coefficient (μ), the density of the material (ρ) and the thickness (d).

$$I = I_{air} e^{-\mu \rho(x,z) d} \tag{1}$$

Relative density (ρ_r) (density of the foamed sample divided by the density of the solid polymer) of the evolving sample can be calculated after applying a logarithmic conversion to Eq. 1. Given that the thickness of the foam is constant and equal to that of the TPU solid pellet used for calibration, it is possible to propose two equations like Eq. 1. One of the equations refers to the attenuation suffered by the incident X-ray beam (I_{air}) by solid polyurethane (I_{TPU}), and another to the evolving foam (I_f). After equalizing both equations, it is possible to obtain the relative density of the foam using (Eq. 2).

$$\rho_r = \frac{log\left(\frac{I_f}{I_{air}}\right)}{log\left(\frac{I_{TPU}}{I_{air}}\right)} \tag{2}$$

For the determination of the cell size evolution (Φ) during the foaming process, every image that conforms the radioscopy has been analysed following a sequential process. First of all, the images are scaled to convert pixels into distances. Afterwards, a minimum filter is applied to enhance the darker solid phase pixels (solid phase is more X-ray absorbing). Then, automatic binarization of the radioscopy images was performed. As transmitted intensity through the sample increases during the foaming (meanwhile the relative density decreases), the threshold limits for the binarization of the image increase automatically with the monitored time. Afterwards, a watershed segmentation algorithm is applied to create the cell walls that separate pores. The resulting masks (binarized images) are analysed by a size and roundness selective procedure which enables to remove noise and other artefacts from the images.

Finally, the evolution of cell nucleation density [32] can be calculated according to Eq. 3 employing the measured values of relative density and cell size evolution.

$$N_o = \frac{6}{\pi \Phi^3}\left(\frac{1}{\rho_r} - 1\right) \tag{3}$$

2.2.5 Kinetic studies

Reaction kinetics for the reference material (Reference) and the materials containing 1 wt% aerogel (1% A) and 3 wt% aerogel (3% A) were studied. To this end, two different techniques were employed: *in-situ* FTIR [5,33] and reaction temperature evolution measurements [5].

In-situ FTIR spectra of the samples were collected using a Bruker ALPHA spectrometer by attenuated total reflectance (ATR) method [5,33]. From the 50 g reacting mixture (section 2.2.1), 1 mL was extracted and poured on the surface of the ATR cell. The FTIR experiments lasted 30 minutes, during this time 60 spectra were acquired, one every 30 s. The temperature of the experiment was set at 70ºC. In addition, to monitor the amount of reaction products of the blowing and polymerization reaction a deconvolution of the amide I region (carbonyl region) was carried out as indicated in the literature [33–35].

The reaction temperature evolution during the foaming process was also measured. Three thermocouples (type K) were introduced in a plastic cup of 11.5 cm of diameter and 14 cm of height to measure the temperature during 60 minutes at three different positions. Three thermocouples were placed vertically in the centre of the plastic cup at the following heights from the base of the cylinder: 0.5 cm (thermocouple 1, T1), 2.0 cm (thermocouple 2, T2) and 6.5 cm (thermocouple 3, T3). The data collected by the thermocouples were registered with a computer. Three experiments were performed for each material.

3 Results and discussion

3.1 Aerogel powder characterisation

FTIR spectra of the silica aerogel particles can be observed in Fig. 3. The strong absorption bands appearing at 1047.74 cm^{-1} and 841.77 cm^{-1} are the characteristic peaks of the asymmetric and symmetric stretching vibration of Si-O-Si, respectively [33,36–38]. On the other hand, the absorption peak located at 1254.49 cm^{-1} is due to the CH_3 deformation in the bond Si-CH_3 [39]. Moreover, the peak intensity detected at 2962.67 cm^{-1} and 756.46 cm^{-1} can be attributed to the C-H stretching and bending vibration, respectively. These weaker peaks confirm the existence of methyl groups belonging to the superficial treatment of the aerogel powder (Fig. 1b). Thus, the FTIR spectra confirm the presence of hydrophobic groups on the surface of the particles. The hydrophobic nature of aerogel can also be verified by the absence of the characteristic peak for the Si-OH bond in silica aerogel (~1630 cm^{-1})[37].

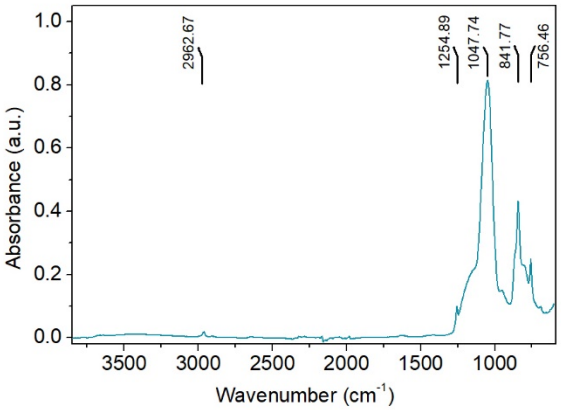

Fig. 3: FTIR spectra of the Enova® Aerogel powder.

The particle morphology has been examined using high-resolution SEM imaging, as seen in Fig. 4. The micrographs (Fig. 4 a) reveal the micrometric size of the particles. As it can be observed in this figure, the majority of the particles have sizes close to 15 µm supporting the data provided by the supplier. Concerning the nanoporous structure of the particles, it is possible to appreciate in Fig. 4 b a textured surface of the particles. Moreover, darker areas on the surface resemble pores or holes on this surface, with sizes in the range of 15 nm.

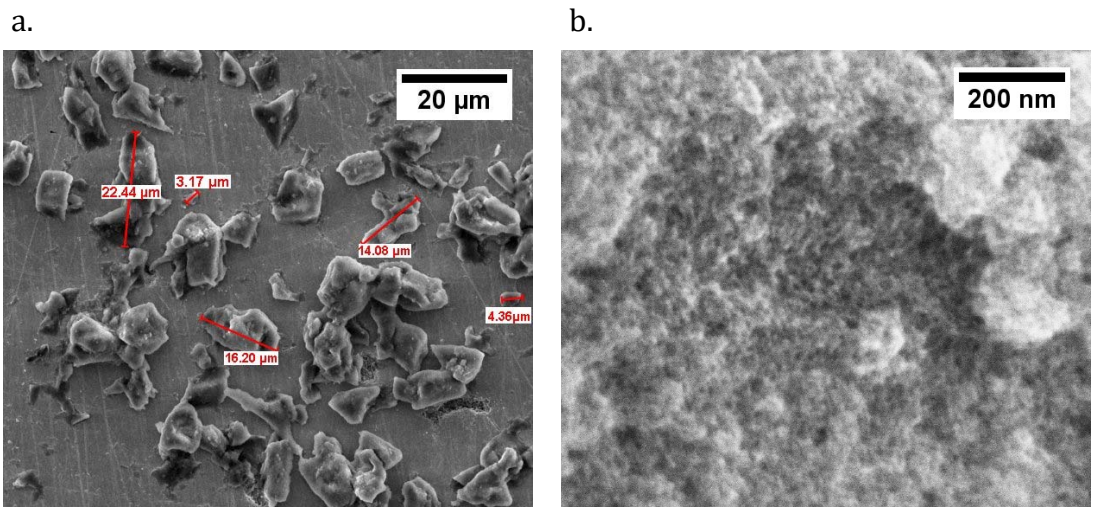

Fig. 4: a. SEM micrographs of the Enova® Aerogel powder dissolved in ethanol, b. SEM micrograph of the Enova® Aerogel particles surface.

3.2 Foam density, cell size and open cell content characterisation

To verify the evolution of foam density and cell size with increasing aerogel content the final geometric density and cell size of all foams were investigated and are gathered in Table 1. Average cell size values were obtained from the equivalent sphere diameter of the cell volumes measured by means of X-ray Tomography (Fig. 5) [30]. Moreover, SEM micrographs were acquired of the foams' growth plane and are shown in Fig. 6.

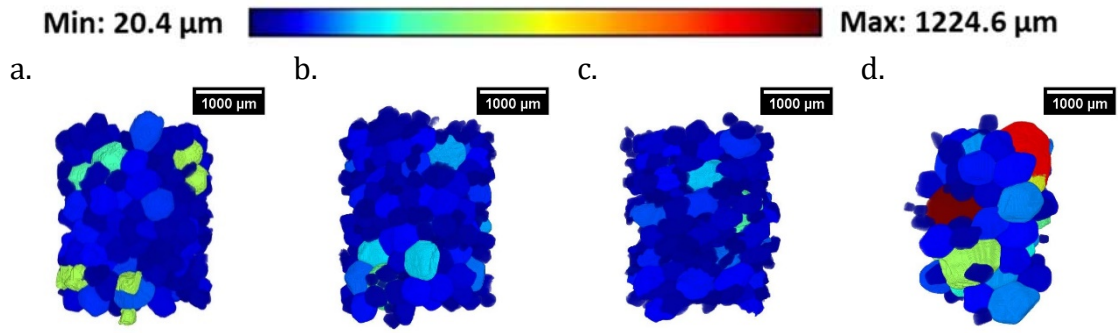

Fig. 5: 3D renderings of the X-ray tomography scanned volumes colored according the displayed color-size scale (upper row). a. Reference, b. 0.5% A, c. 1% A and d. 3% A.

Table 1 shows that the foam containing 3 wt% silica aerogel (3% A) has a similar density to that of the reference foam (Reference). In contrast, the foams with 0.5 wt% and 1 wt% silica aerogel (0.5% A and 1% A) present a slight increase in density with respect to Reference foam (only around 5% increase). Therefore, the introduction of silica aerogel fillers does not significantly alter the density of the RPU cured foam.

Table 1: Density, relative density and open cell content for every foam manufactured.

Material	Density (kg/m³)	Relative density	Open cell content (%)	Cell Size (µm)
Reference	38.1 ± 0.5	0.033	6.1 ± 0.1	412.5 ± 122.7
0.5% A	40.3 ± 0.1	0.035	7.5 ± 0.4	309.6 ± 180.0
1% A	39.8 ± 0.8	0.034	8.4 ± 1.6	290.7 ± 168.3
3% A	38.2 ± 0.4	0.033	19.8 ± 3.5	454.7 ± 234.1

On the other hand, the evolution of the open cell content with aerogel concentration has also been studied, as shown in Table 1. The influence of aerogel silica powder in this magnitude is evident. Open cell content of the RPU foams shows an increase with the addition of aerogel; this effect is the most visible for sample 3% A.

In contrast, the average cell size progressively decreases when low contents of particles (below 1 wt%) are added to the polyurethane matrix, reaching a reduction near the 30% for the foam containing 1% of silica aerogel. Whereas, it slightly increases when 3 wt% of aerogel is used. The cell size for this material is similar to that of the reference material.

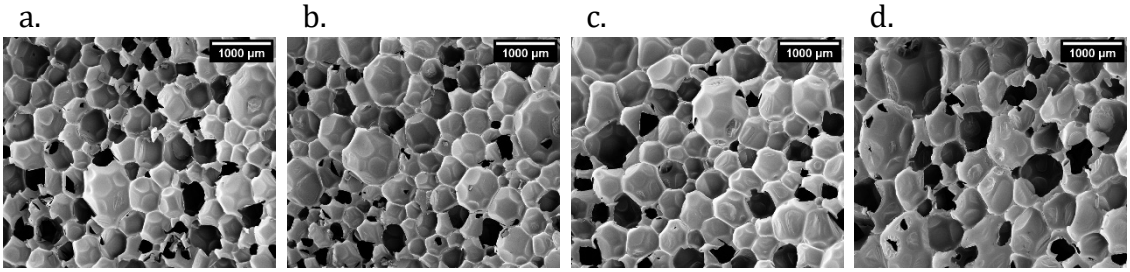

Fig. 6: SEM micrographs of a. Reference, b. 0.5% A, c. 1% A and d. 3%A.

3.3 Foaming behaviour

3.3.1 Relative density evolution

Fig. 7 shows curves for the relative density evolution during foaming. These results are plotted to take as the initial time the beginning of the isocyanate and polyol stirring process. Therefore, all curves present a time span of 66.4 seconds that results from the time required to perform the mixture of the polyol with isocyanate, position the RPU drop inside the foaming frame (Fig. 2b) and introduce the sample inside the X-ray cabinet. Therefore, the beginning of the experiments occurs once the foam rise has already started. The first radiography is acquired approximately 10 seconds after the cream time, which is 50 seconds.

Fig. 7 reveals how, during the firsts instants of the foaming process, a rapid density decrease takes place, as a consequence of the CO_2 gas generated during the blowing reaction [11]. After that, the expansion rate is reduced due to a combination of polymerization evolution (increasing the material viscosity) and the reduced amount of gas generated at long times. Attending to the differences observed among curves, Fig. 7 shows how the inclusion of a small amount of these nanoporous particles (0.5 and 1 wt%) slightly increases the density of the aerogel filled foams with respect to the reference at any time during the process. Furthermore, when a higher content in aerogel particles (3 wt%) is introduced into the foam, its density evolution trend is altered, ending with a density similar to the reference despite showing a higher density at short reaction times.

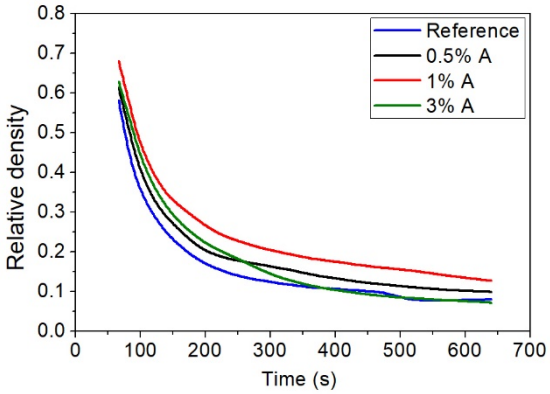

Fig. 7: Representative curves of the relative density evolution versus time of the reference and aerogel composite foams.

In addition, when observing the slopes of the relative density evolution process (Fig. 8), it is detected how at short times Reference material shows a remarkably rapid density decrease, whereas composite foams present a slower evolution. Nevertheless, this trend shifts at times higher than 95 seconds (Fig. 8b). At longer

times, the foams reinforced with aerogel particles decrease their density more readily. Despite this, at the end of the radioscopy experiments, the foams with 0.5 wt% and 1 wt% of aerogels end with higher relative density values than the reference.

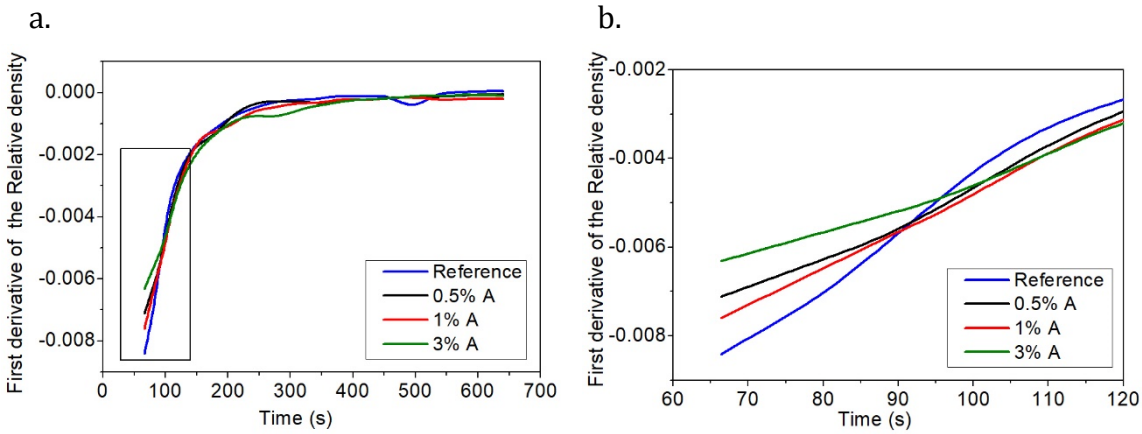

Fig. 8: a. Relative density decreasing speed versus time for reference foam and aerogel composite foams (0.5% A, 1% A and 3% A). b. Zoom of the previous figure at short reaction times.

Furthermore, the accuracy of the relative density values obtained by radioscopy has been confirmed by measuring the density (Table 1) of the cured foams. Table 1 and Fig. 7 at long times show similar results. Both results reveal how the addition of low contents of aerogel (0.5 wt% and 1 wt%) increases the density of the foams, however, when high contents (3 wt%) are employed the density of the foam remains similar to the density of the unfilled foam.

3.3.2 Cell size evolution

A visual comparison between the cellular structure of the four composite foams can be appreciated in Fig. 9. The main changes in cellular structure are observed at two stages of the foam evolution, after the onset of foam rise, 84 s, and once the cellular structure is almost solidified, 580 s. Between these two foaming stages the growth of the cells can be appreciated. In addition, the increase in grey level intensities observed between foams at 84 s and 580 s is related to the reduction in density reported previously (Fig. 7). At early stages, it is challenging to appreciate clear differences from a simple visual inspection. However, at the final stages of the foaming, 580 s, the composite sample with 3 wt% aerogel shows a cellular structure with remarkably larger pores (ca. 1 mm) than reference foam and those foams with 0.5 wt% and 1 wt% silica aerogel.

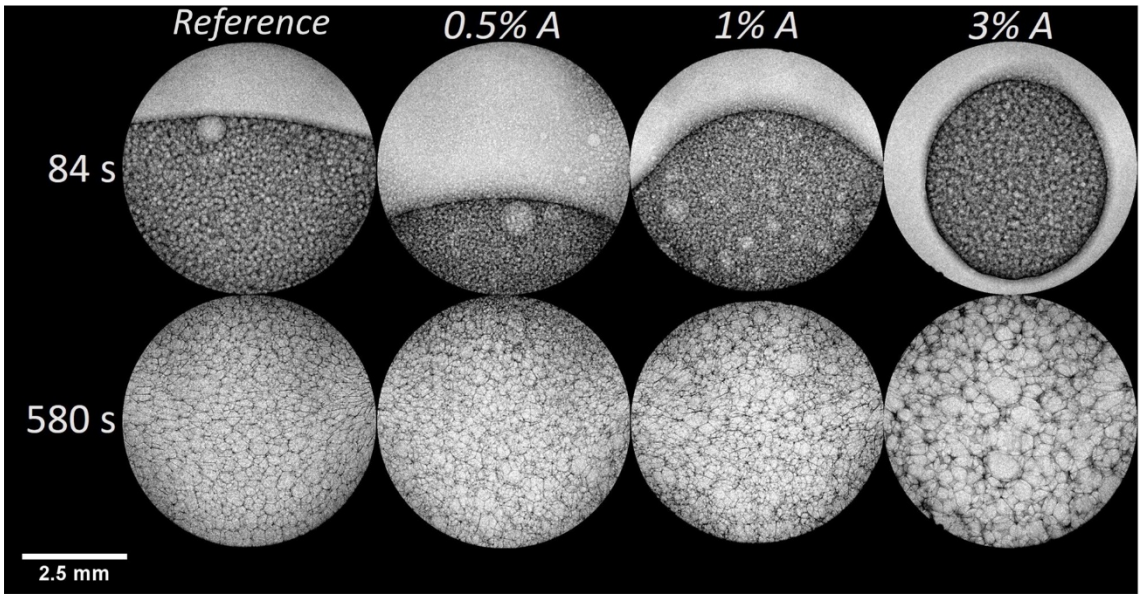

Fig. 9: X-ray radiographs of expanding reference and aerogel composite foams at the beginning and ending of the foaming process.

The qualitative observations that can be extracted from Fig. 9 are confirmed when analysing the radioscopy sequences (Fig. 10 a). A dissimilar pore-growing slope for the different materials is observed. During the foam rise, cell growth rate (Fig. 10 b) is exceptionally high in the case of the foam with 3 wt% of aerogel (60-120 seconds), reaching cell size growing speeds of 3 µm/s. Such expansion rate is not achieved by any other sample. Reference foam reaches cell size expansion speed close to 2 µm/s whereas composites with low content in aerogel, 0.5 wt%, and 1 wt%, show a rather slow cell growth rate (below 1.5 µm/s). Furthermore, they present a remarkable cell size reduction compared to the reference at the end of the foaming process. On the other hand, sample 3% A, which starts the foaming process with the smallest cell size, shows the largest pore size at the end of the monitored time due to this quick increase of cell size with time.

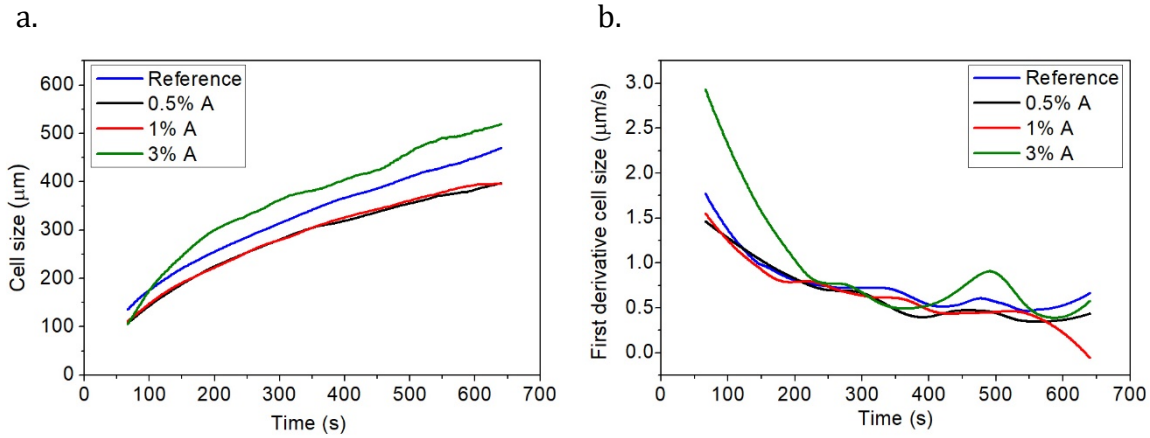

Fig. 10: a. Cell size evolution with time and b. Cell size growing speed for all the RPU foams under study

The quick transition from small to larger pores in the case of sample 3% A can be interpreted as a sign of cellular structure instability, i.e. presence of cellular degeneration mechanisms such as coalescence [40]. This mechanism is characterised by the cell wall rupture between adjacent cells, leading to the junction of small-sized cells into bigger ones, especially at low densities when cell walls are thinner [41]. The cellular instability detected here matches the increase in open cell content observed as the content in aerogel increases, Table 1. This effect was extremely remarkable for the sample containing 3 wt% of aerogel particles, reaching almost 20% of open cell content. On the other hand, it is also interesting to observe that the cell size of samples containing 0,5% or 1% aerogel is reduced at the end of the experiment (same result to that found in Table 1). Mainly as a consequence of the lower cell size at early stages and a slower increase of cell size with time.

3.3.3 Cell nucleation density evolution

The obtained results exhibit a fluctuating behaviour depending on the filler amount in the materials (Fig. 11).

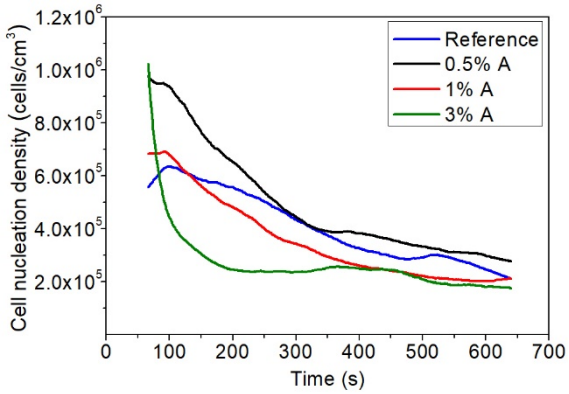

Fig. 11: Cell nucleation density evolution with time for all the foams manufactured.

Initially, the presence of aerogel particles increases the number of nucleation sites with respect to the reference, as described by classical nucleation theories [42]. Even though the nucleation process occurred before the monitoring began, it is possible to confirm this effect due to the higher cell nucleation density of the aerogel-filled foams immediately after the foam rise starts. Moreover, the cell density does not stay constant with time in any of the composite foams though in some cases Reference, 0.5% A and 1% A the variations are small. As it was reported for material 3% A, the swift increase in cell size together with the reduction in cell nucleation density is a clear symptom of cell degeneration mechanisms. These cell degeneration processes prevail at long times over the enhanced nucleation experienced by the composite foams. A possible explanation for these degeneration phenomena could be the broad particle size range of Enova® Aerogel powder (Fig.

4 a) and the high content of particles in this particular system. Fillers are usually hosted in the struts and cell walls of the foam. However, particles with sizes close to 40 μm, could undoubtedly cause cell walls (with thickness around 1-2 μm) to weaken and break, leading to the joining of adjacent cells and increasing of the open cell content (Table 1).

3.4 Kinetic study

As it was previously commented, the RPU foam formation is a consequence of a reactive foaming process between isocyanate with water (blowing reaction) and polyol (polymerization reaction). The addition of particles to the RPU formulation can alter the rates of conversion of isocyanate and modify the balance between the generation of urethane and urea products. This type of information is vital to understand the observed changes in the foaming behaviour of RPU when different contents in aerogel particles are introduced. As observed in Fig 7 and Fig 10, the relative density and cell size evolution of foams 0.5% A and 1% A are essentially analogous. What is more, their final cellular structure and density also agree (see section 3.2). For these reasons, foam 0.5% A was excluded from this analysis on the assumption that foams with low aerogel contents present the same foaming behaviour. Therefore, the kinetic study discussed below was then performed for the foams Reference, 1% A and 3% A.

3.4.1 FTIR Measurements

The isocyanate consumption can be evaluated with the decrease of the isocyanate asymmetric stretching vibration at 2270 cm^{-1}. In contrast, the generation of urethane and urea products are followed, considering the increase of the carbonyl stretching vibrations of the Amide I Region in the range 1610–1760 cm^{-1}[5].

Firstly, during foaming, the isocyanate group conversion (pNCO) is quantified by the decay (Eq. 4) of the isocyanate absorption band; located between 2500 and 2000 cm^{-1}[43]:

$$pNCO = \frac{A_0 - A_{max}}{A_0} \quad (4)$$

In Eq. 4 A_0 represents the absorbance of the isocyanate band for the first acquired spectra, and A_{max} is the integrated absorbance of the isocyanate band at time ~ 0 [5]. Fig. 12 shows curves for the isocyanate conversion of foams Reference, 1% A and 3% A. It is clear how the foam with the highest content in aerogel particles presents the highest isocyanate consumption, followed by the reference. However, as

observed in the relative density evolution curves (Fig. 7), there is not a linear trend in the monitored magnitudes with the addition of aerogel particles. In fact, 3% A and Reference show a similar isocyanate consumption and relative density evolution (at the last minutes of the foaming process). Whereas, 1% A presents low values of isocyanate consumption during the complete foaming process. Previous works have noted that depending on the filler content the isocyanate reaction is conditioned either by the viscosity of the initial mixture or the particle characteristics [10,33,44]. For low amounts of fillers, the reaction rate is dominated by the viscosity increase. Thus, the addition of 1 wt% of aerogel could increase the viscosity of the isocyanate part triggering a reduction in the mobility of the reacting chains and a smaller isocyanate conversion. Whereas, when high amounts are employed is the fillers' surface treatment which strongly conditions the reaction rates. Since aerogel particles have a hydrophobic surface treatment that does not interact with the OH groups coming from the polyol or water, the isocyanate consumption is enhanced [33]. However, for all foams, it is clear how the isocyanate consumption increases rapidly (in less than 200 seconds) to almost its maximum value observed in the 30 minutes monitored by *in-situ* FTIR spectra.

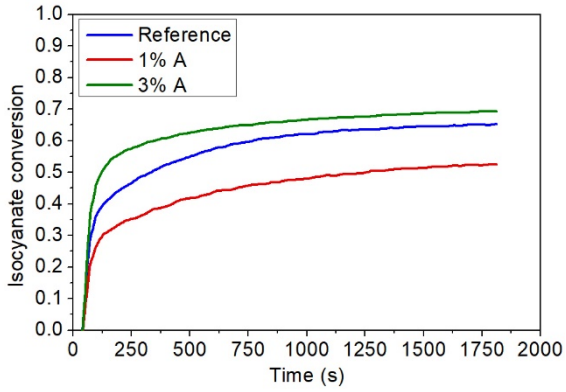

Fig. 12: Average isocyanate conversion versus time for foams Reference, 1% A and 3% A.

The rate of generation of products can be obtained from the deconvolution of the Amide I region of the acquired spectra. This procedure permits separating the different carbonyl groups present in the reaction mixture and obtaining the relative area percentages of ureas and urethanes [35,36]. Relative area percentages of products generated at different times are obtained by dividing the corresponding peak area by the total Amide I area (summing up the areas of all peaks present in this carbonyl region). From this, the urethane/urea ratio at different times is calculated from the relative area percentages of urethanes groups divided by the relative area percentages of ureas groups (Fig. 13). From Fig. 13, it is clear how the reaction kinetics of 1% A are strongly affected by the presence of aerogel, increasing the generation of urethane products with respect to ureas during the whole foaming

time. Nevertheless, this trend is not preserved when higher amounts of aerogel are used. 3% A shows a similar behaviour than that of the reference sample.

These results indicate how the addition of low aerogel contents seems to favour the polymerization during the first minutes of foaming. All in all, the trend followed by foams ratio of urethane/urea is very similar to that observed for the relative density evolution. When the polymerization reaction is favoured, as it is the case of foam containing 1 wt% aerogel, the increase in density is significant because the urethane formation is quicker. Thus, the viscosity is higher during early stages of foaming, giving as a consequence a lower expansion ratio. Meanwhile, a higher amount of ureas, as it is the case of foam 3% A, involves higher CO_2 generation and therefore, a more substantial density decrease.

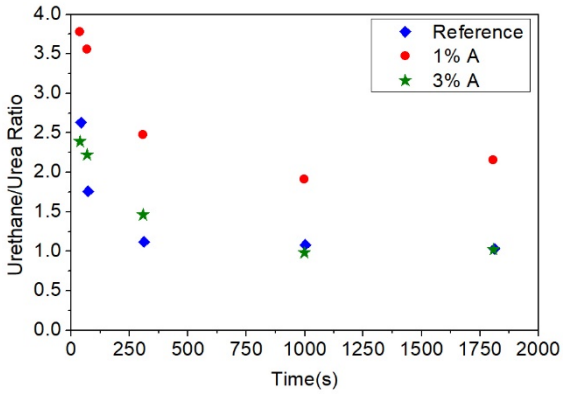

Fig. 13: Relative area percentage of the absorbances of urea or urethane detected in the Amide I region at different stages of the foaming process.

3.4.2 Reaction temperature measurements

The reactions responsible for the generation of RPU foams, polymerization and blowing, are both exothermic. The heat liberated in the polymerization reaction is approximately 24 kJ/mol of urethane formed, while the blowing reaction releases 47 kJ/mol of urea generated [45]. During the formation of RPU, the centre of the foam is isolated from its surroundings, making it comparable to an adiabatic system.

Fig. 14 represents the temperature reached by the foams Reference, 1% A and 3% A, versus time at different heights during its growing process. As it can be observed from the data reported in Table 2, Reference shows higher peak temperatures in all the measured regions of the foams. The higher temperature of the reference is the most remarkable for the upper areas of the foam, near the top, where the temperature recorded by the medium thermocouple inside the reference foam is on average 3.5 ºC higher than for the composite foams. There are also some significant differences when it comes to the time of reaction needed to reach the peak temperature. It is appreciated how the foam 3% A reaches its maximum internal

temperature sooner than the reference and 1% A foams (on average around 1 minute before).

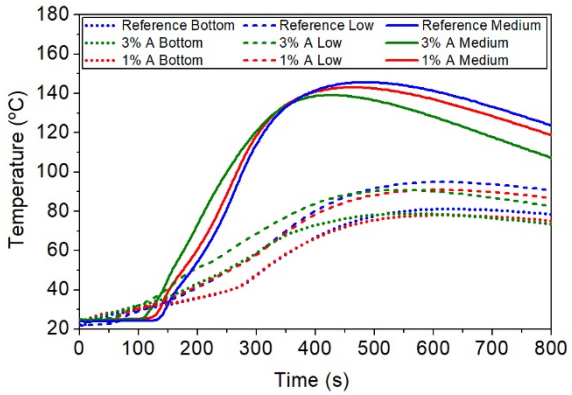

Fig. 14: Temperature evolution during the foaming process detected by thermocouples for all the analysed samples.

Furthermore, since the reaction temperatures have been measured for sixty minutes, it is possible to monitor the temperatures during the cooling down process of the foam, as it progressively equilibrates its temperature to that of its surroundings. Thus, it is also possible to determine the heat dissipation speed of each foam as it cools down (Table 3). This cooling down rate has been calculated as the slope of the temperature decrease during twelve minutes from the maximum temperature registered.

Table 2: Maximum temperatures and time to reach them for the foams Reference, 1% A and 3% A.

Material	Bottom: Peak (ºC)	Bottom: Peak time (s)	Low: Peak (ºC)	Low: Peak time (s)	Medium: Peak (ºC)	Medium: Peak time (s)
Reference	81.2 ± 2.3	625.3 ± 15.3	94.9 ± 2.1	611.7 ± 11.4	145.7 ± 1.8	483.3 ± 11.8
1% A	78.1 ± 1.0	612.5 ± 12.0	91.0 ± 1.1	609.0 ± 5.7	143.1 ± 1.1	458.5 ± 6.4
3% A	80.5 ± 2.2	534.5 ± 137.9	92.7 ± 2.9	539.5 ± 143.5	141.4 ± 2.8	420.5 ± 84.1

Table 3 reveals that 3% A has higher heat dissipation speeds in all areas in which the temperature has been monitored. The swifter dissipation speed of this foam is related to its elevated cell opening in contrast with the low open cell content of foams filled with fewer aerogel particles (Table 1). This cell opening also explains why 3% A seems to reach a lower internal temperature despite presenting the highest isocyanate conversion.

Table 3: Heat dissipation speed for the RPU foams containing 0 wt%, 1 wt% and 3 wt% of aerogel.

Material	Bottom: Temperature Cooling Speed (ºC/s)	Low: Temperature Cooling Speed (ºC/s)	Medium: Temperature Cooling Speed (ºC/s)
Reference	-0.027 ± 0.0006	-0.036 ± 0.0005	-0.078 ± 0.0013
1% A	-0.024 ± 0.0004	-0.035 ± 0.0016	-0.078 ± 0.0004
3% A	-0.031 ± 0.0049	-0.038 ± 0.0011	-0.093 ± 0.0011

3.5 Discussion

Cell nucleation power of aerogel particles has been demonstrated thanks to X-ray radioscopy. During the early stages of foaming higher cell nucleation density has been observed for all the aerogel concentrations tested (Fig. 11). We have detected how the introduction of micro-sized aerogel particles also induces degeneration of the cellular structure. In the radioscopy sequences, it is appreciated that degeneration shows up as coalescence, which causes a significant reduction in the number of cells and increases the rate of cell growth as it can be seen in Fig 10. After a few minutes, when the foam expansion is almost completed, low aerogel content composite foams present a reduction of cell size with regard to the reference (around 16%). Meanwhile, the foam with a 3 wt% of aerogel particles suffers the strongest degeneration, showing at the end of the experiment cell sizes 10% larger than the reference. These modifications in the cellular structure with the addition of aerogel are confirmed in the large foams produced with 50 g of material (Section 2.2.1). In the cured samples 0.5% A and 1% A a reduction of approximately 26% has been measured, whereas 3% A reveals a 10% increase in its average cell size (Table 1). Consequently, in foams with low contents of aerogel, the final cell size is reduced with respect to Reference because nucleation prevails over coalescence in these systems. Whereas, in foams with high contents of aerogel the size and number of these particles boost degeneration which prevails over nucleation leading to a material with larger cells than the reference.

The onset of degeneration mechanisms can be explained when considering the reaction products. The results of Fig. 13 indicate that foams Reference and 3% A follow similar product balance during the monitored time. Both begin with a superior number of urethane products, but after a few minutes, the amount of urethane and urea products equates. We hypothesise that when cells impinge the matrix is still highly viscous, and the presence of large particles induces significant cell wall instability: promoting drainage of material from the cell walls to the struts and ruptures of the walls. Besides, it is to be noted that employing a 3 wt% of aerogel (particle density 150 kg/m^3) entails introducing into the foam a considerable number of particles, around $7 \cdot 10^9$ particles in total –assuming that they have an average diameter of 15 μm. Considering that for a foam of 40 kg/m^3, average cell density is close to $5 \cdot 10^3$ cells/cm^3 and that cells are shaped like pentagonal dodecahedrons there will be no more than $3 \cdot 10^4$ struts/cm^3, it is clear that the majority of particles will be agglomerated in the struts since they are unlikely to be hosted in the cell walls.

On the other hand, the kinetic balance changes significantly when 1 wt% of aerogel is added. In this case, for the whole experiment time, an enhancement of the

polymerization reaction (generation of more urethane products) is detected. In turn, an effective cell size reduction is reached, both in the in-situ experiment and in the large-sized foam. A possible rationale to explain this fact may be that a stronger polymerization promotes a swifter cellular structure stabilization. Then the polymer matrix vitrifies more readily, and hence the material that forms the walls attains higher viscosity in less time, making drainage and coalescence events less likely.

Relative density results at initial stages (60 s-150 s) show how aerogel delays the foam expansion. This fact is probably a consequence of the isocyanate's viscosity increase due to the presence of aerogel particles and the enhancement of the polymerization reaction (rise in the number of urethane groups) as observed by *in-situ* FTIR spectroscopy. In the final stages (t>5 min) and final foam Reference and 3% A present comparable expansion (physical interaction) which might be motivated by the similar isocyanate conversion (Fig. 12) and number of products (chemical interaction) measured in both materials (Fig. 13). Yet, foams filled with small amounts of aerogel achieve lower expansion ratio because they undergo a swifter and more intense polymerization (as in-situ measured for foam 1% A). This explains why materials such as 0.5% A and 1% A end the foaming process with a slightly higher density than foams filled with higher aerogel contents.

The relationship between isocyanate conversion and reaction temperature has been studied in previous works [5,45]. It has been proposed that higher internal temperature during foaming may be linked to an increase in the isocyanate consumption and thus, a higher number of products generated. From Fig. 14, it can be appreciated how the foams internal temperature drops with increasing content of particles. Even when the highest consumption of isocyanate was found for foam 3% A followed by Reference and 1% A. Yet, the higher content of open porosity (around 20%) of material 3% A might be acting as an aid for rapid heat dissipation speed to the surroundings (Table 3) and consequently overshadowing the real internal temperature reached by this foam. This hypothesis is also supported by the time taken by each material to attain its peak temperature. In essence, 3% A takes on average 1 minute less than the foams with less open cell content. Thus, the faster temperature increase is in good agreement with the higher reaction speed as measured by FTIR spectroscopy.

4 Conclusions

The foaming evolution of aerogel RPU composite foams was investigated by X-ray radioscopy, FTIR spectroscopy and internal temperature evolution. The influence of aerogel particles on the cellular structure and polyurethane chemical reactions has

been studied for the first time using *in-situ* experiments. Relative density evolution is slowed down by the presence of aerogel. The results at early stages also point out to the cell nucleation power of aerogel particles. Cell size evolution is strongly conditioned by the interaction of the particles with the natural reaction kinetics of Reference. Concentrations of aerogel above 1 wt% speed up and enhance the reactivity of the system. Large amounts of aerogel promote substantial coalescence. Particles, bigger than the polymeric matrix features (walls ~2 μm and struts > 15 μm [30]), act as spots for cell wall ruptures; increasing the generation of holes in the cell walls. These holes may act as sinks for heat dissipation and drive to low cell densities in the final foam. However, there is an optimum content of 1 wt% of aerogel that reduces the final foam cell size by boosting the polymerization, which in turn diminishes the number of cell walls ruptures and open cells.

All these results give valuable insight into the modifications suffered by an RPU formulation (Reference) when an external solid additive (aerogel micrometric particles) is dispersed into the raw materials before the foaming. The results obtained in this work can provide strategies to improve the formulations so that larger amounts of particles can be dispersed into the material producing at the same time good quality foams. On the one hand, the formulation could be modified to increase the polymerization reaction speed for all particle contents employing dedicated catalysts and surfactants, and hence preserving the increases in cell nucleation density. On the other hand, the presence of particles bigger than a few microns most certainly fosters cell wall ruptures since most of these particles only fit into the struts.

Regarding the discussion on the number of struts and powder size (section 3.5), it is clear that the particles will inevitably form aggregates. Good dispersion of particles in the matrix is essential when looking to reinforce the material's properties. Therefore, to maximize the benefits of incorporating aerogel, the particle size should be trimmed so that they can also be hosted in the walls and not only agglomerated in the struts.

CRediT authorship contribution statement

Paula Cimavilla-Román: Conceptualization, Data curation, Investigation, Software, Methodology, Formal analysis, Writing - original draft. **Saúl Pérez-Tamarit**: Conceptualization, Data curation, Investigation, Software, Formal analysis, Writing - Review & Editing. **Mercedes Santiago-Calvo**: Conceptualization, Data curation, Investigation, Formal analysis, Writing - Review & Editing. **Miguel Ángel Rodríguez-Pérez**: Conceptualization, Resources, Supervision, Project administration, Funding acquisition, Writing - Review & Editing.

Declaration of Competing Interest

The authors declare that there is no conflict of interest regarding the publication of this article.

Acknowledgements

Financial assistance from the Junta of Castile and Leon (VA275P18) and Spanish Ministry of Science, Innovation and Universities (RTI2018-098749-B-I00) is gratefully acknowledged. Authors thank Cabot Corporation for supplying us with Enova® Aerogel IC3100 powder. Financial support from Junta de Castilla y Leon predoctoral grant of P. Cimavilla-Román, co-financed by the European Social Fund is acknowledged.

Data availability statement

The raw/processed data required to reproduce these findings cannot be shared at this time as the data also forms part of an ongoing study.

References

[1] L. Chen, L.S. Schadler, R. Ozisik, An experimental and theoretical investigation of the compressive properties of multi-walled carbon nanotube/poly(methyl methacrylate) nanocomposite foams, Polymer (Guildf). 52 (2011) 2899–2909. doi:10.1016/J.POLYMER.2011.04.050.

[2] X. Han, C. Zeng, L.J. Lee, K.W. Koelling, D.L. Tomasko, Extrusion of polystyrene nanocomposite foams with supercritical CO2, Polym. Eng. Sci. 43 (2003) 1261–1275. doi:10.1002/pen.10107.

[3] J.Q. Wang, W.K. Chow, A brief review on fire retardants for polymeric foams, J. Appl. Polym. Sci. 97 (2005) 366–376. doi:10.1002/app.21758.

[4] S. Estravís, J. Tirado-Mediavilla, M. Santiago-Calvo, J.L. Ruiz-Herrero, F. Villafañe, M.A. Rodríguez-Pérez, Rigid polyurethane foams with infused nanoclays: Relationship between cellular structure and thermal conductivity, Eur. Polym. J. 80 (2016) 1–15.

[5] M. Santiago-Calvo, V. Blasco, C. Ruiz, R. París, F. Villafañe, M.-Á. Rodríguez-Pérez, Synthesis, characterization and physical properties of rigid polyurethane foams prepared with poly(propylene oxide) polyols containing graphene oxide, Eur. Polym. J. 97 (2017) 230–240.

[6] O.A. Almanza, M.A. Rodriguez-Perez, J.A. De Saja, Prediction of the radiation term in the thermal conductivity of crosslinked closed cell polyolefin foams, J. Polym. Sci. Part B Polym. Phys. 38 (2000) 993–1004.

[7] L.J. Lee, C. Zeng, X. Cao, X. Han, J. Shen, G. Xu, Polymer nanocomposite foams, Compos. Sci. Technol. 65 (2005) 2344–2363.

doi:10.1016/j.compscitech.2005.06.016.

[8] M. Szycher, Szycher's handbook of Polyurethanes, Second edi, Taylor & Francis Group, London, 2013. doi:10.1038/142853a0.

[9] S. Pardo-Alonso, E. Solórzano, S. Estravís, M. a. Rodríguez-Perez, J. a. de Saja, In situ evidence of the nanoparticle nucleating effect in polyurethane–nanoclay foamed systems, Soft Matter. 8 (2012) 11262. doi:10.1039/c2sm25983d.

[10] M.M. Bernal, M.A. Lopez-Manchado, R. Verdejo, In situ foaming evolution of flexible polyurethane foam nanocomposites, Macromol. Chem. Phys. 212 (2011) 971–979. doi:10.1002/macp.201000748.

[11] M. Mar Bernal, S. Pardo-Alonso, E. Solórzano, M.Á. Lopez-Manchado, R. Verdejo, M.Á. Rodriguez-Perez, Effect of carbon nanofillers on flexible polyurethane foaming from a chemical and physical perspective, RSC Adv. 4 (2014) 20761. doi:10.1039/c4ra00116h.

[12] A. Kausar, Polyurethane Composite Foams in High-Performance Applications: A Review, Polym. - Plast. Technol. Eng. 57 (2018) 346–369. doi:10.1080/03602559.2017.1329433.

[13] M.C. Saha, M.E. Kabir, S. Jeelani, Enhancement in thermal and mechanical properties of polyurethane foam infused with nanoparticles, Mater. Sci. Eng. A. 479 (2008) 213–222. doi:10.1016/j.msea.2007.06.060.

[14] S.H. Kim, M.C. Lee, H.D. Kim, H.C. Park, H.M. Jeong, K.S. Yoon, B.K. Kim, Nanoclay reinforced rigid polyurethane foams, J. Appl. Polym. Sci. 117 (2010) 1992–1997. doi:10.1002/app.32116.

[15] S. Pardo-Alonso, E. Solórzano, M.A. Rodriguez-Perez, Time-resolved X-ray imaging of nanofiller-polyurethane reactive foam systems, Colloids Surfaces A Physicochem. Eng. Asp. 438 (2013) 119–125.

[16] J. Li, X. Mo, Y. Li, H. Zou, M. Liang, Y. Chen, Influence of expandable graphite particle size on the synergy flame retardant property between expandable graphite and ammonium polyphosphate in semi-rigid polyurethane foam, Polym. Bull. (2018) 1–18. doi:10.1007/s00289-018-2309-y.

[17] W. Wang, H. Pan, B. Yu, Y. Pan, L. Song, K.M. Liew, Y. Hu, Fabrication of carbon black coated flexible polyurethane foam for significantly improved fire safety, RSC Adv. 5 (2015) 55870–55878. doi:10.1039/c5ra06170a.

[18] C. Zhao, Y. Yan, Z. Hu, L. Li, X. Fan, Preparation and characterization of granular silica aerogel/polyisocyanurate rigid foam composites, Constr. Build. Mater. 93 (2015) 309–316. doi:10.1016/j.conbuildmat.2015.05.129.

[19] A. Dourbash, C. Buratti, E. Belloni, S. Motahari, Preparation and characterization of polyurethane/silica aerogel nanocomposite materials, J. Appl. Polym. Sci. 134 (2017) 1–13. doi:10.1002/app.44521.

[20] N. Nazeran, J. Moghaddas, Synthesis and characterization of silica aerogel reinforced rigid polyurethane foam for thermal insulation application, J. Non. Cryst. Solids. 461 (2017) 1–11. doi:10.1016/j.jnoncrysol.2017.01.037.

[21] M. Martin-Gallego, M.M. Bernal, M. Hernandez, R. Verdejo, M.A. Lopez-Manchado, Comparison of filler percolation and mechanical properties in

graphene and carbon nanotubes filled epoxy nanocomposites, Eur. Polym. J. 49 (2013) 1347–1353. doi:10.1016/j.eurpolymj.2013.02.033.

[22] A. Soleimani Dorcheh, M.H. Abbasi, Silica aerogel; synthesis, properties and characterization, J. Mater. Process. Technol. 199 (2008) 10–26. doi:10.1016/j.jmatprotec.2007.10.060.

[23] H. Zhang, Y. Qiao, X. Zhang, S. Fang, Structural and thermal study of highly porous nanocomposite SiO2-based aerogels, J. Non. Cryst. Solids. 356 (2010) 879–883. doi:10.1016/j.jnoncrysol.2010.01.003.

[24] G. Wei, Y. Liu, X. Zhang, X. Du, Radiative heat transfer study on silica aerogel and its composite insulation materials, J. Non. Cryst. Solids. 362 (2013) 231–236. doi:10.1016/j.jnoncrysol.2012.11.041.

[25] E. Solórzano, S. Pardo-Alonso, J.A. De Saja, M.A. Rodriguez-Perez, X-ray radioscopy in-situ studies in thermoplastic polymer foams, Colloids Surfaces A Physicochem. Eng. Asp. 438 (2013) 167–173. doi:10.1016/j.colsurfa.2013.01.043.

[26] Cabot Corporation, Enova Aerogel Fine Particles, Saf. Data Sheet. (2012) 1–8. http://www.buyaerogel.com/wp-content/uploads/2014/02/NGFPA-EUR-EN.pdf.

[27] S. Pardo-Alonso, E. Solórzano, S. Estravís, M. a. Rodríguez-Perez, J. a. de Saja, In situ evidence of the nanoparticle nucleating effect in polyurethane–nanoclay foamed systems, Soft Matter. 8 (2012) 11262.

[28] ASTM D1622-08: Standard Test Method for Apparent Density of Rigid Cellular Plastics, (n.d.).

[29] ASTM D6226-10. Standard Test Method for Open Cell Content of Rigid Cellular Plastics, (n.d.).

[30] S. Pérez-Tamarit, E. Solórzano, A. Hilger, I. Manke, M.A.A. Rodríguez-Pérez, Multi-scale tomographic analysis of polymeric foams: A detailed study of the cellular structure, Eur. Polym. J. 109 (2018) 169–178. doi:10.1016/j.eurpolymj.2018.09.047.

[31] S. Pardo-Alonso, X-Ray Imaging Applied to the Characterization of Polymer Foams ' Cellular Structure and Its Evolution, Universidad de Valladolid. Facultad de Ciencias, 2014.

[32] E. Solórzano, J. Pinto, S. Pardo, F. Garcia-Moreno, M.A. Rodriguez-Perez, Application of a microfocus X-ray imaging apparatus to the study of cellular polymers, Polym. Test. 32 (2013) 321–329. doi:10.1016/j.polymertesting.2012.11.016.

[33] M. Santiago-Calvo, J. Tirado-Mediavilla, J.L. Ruiz-Herrero, M.Á. Rodríguez-Pérez, F. Villafañe, The effects of functional nanofillers on the reaction kinetics, microstructure, thermal and mechanical properties of water blown rigid polyurethane foams, Polymer (Guildf). 150 (2018) 138–149. doi:10.1016/j.polymer.2018.07.029.

[34] D.P. Queiroz, M.N. De Pinho, C. Dias, ATR-FTIR studies of poly(propylene oxide)/polybutadiene bi-soft segment urethane/urea membranes, Macromolecules. 36 (2003) 4195–4200. doi:10.1021/ma034032t.

[35] A. Marcos-Fernández, A.E. Lozano, L. González, A. Rodríguez, Hydrogen bonding in copoly(ether-urea)s and its relationship with the physical properties, Macromolecules. 30 (1997) 3584–3592. doi:10.1021/ma9619039.

[36] H. Sanaeishoar, M. Sabbaghan, F. Mohave, Synthesis and characterization of micro-mesoporous MCM-41 using various ionic liquids as co-templates, Microporous Mesoporous Mater. 217 (2015) 219–224.

[37] P. Wagh, R. Kumar, R. P. Patel, I. K. Singh, S. Ingale, S. Gupta, D. Mahadik, A. Venkateswara Rao, Hydrophobicity Measurement Studies of Silica Aerogels using FTIR Spectroscopy, Weight Difference Method, Contact Angle Method and K-F Titration Method, J. Chem. Biol. Phys. Sci. Volume 5 (2015) page no. 2350-59.

[38] P.B. Wagh, S. V. Ingale, Comparison of some physico-chemical properties of hydrophilic and hydrophobic silica aerogels, Ceram. Int. 28 (2002) 43–50.

[39] L.M. Johnson, L. Gao, C.W. Shields, M. Smith, K. Efimenko, K. Cushing, J. Genzer, G.P. López, Elastomeric microparticles for acoustic mediated bioseparations, J. Nanobiotechnology. 11 (2013).

[40] I. Cantat, S. Cohen-Addad, F. Elias, F. Graner, R. Höehler, O. Pitois, F. Rouyer, A. Saint-Jalmes, Foams: structure and dynamics, First Edit, Oxford University Press, Oxford, 2013.

[41] F. Garcia-Moreno, M. Mukherjee, C. Jiménez, A. Rack, J. Banhart, Metal Foaming Investigated by X-ray Radioscopy, Metals (Basel). 2 (2011) 10–21. doi:10.3390/met2010010.

[42] J.S. Colton, N.P. Suh, Nucleation of microcellular foam: Theory and practice, Polym. Eng. Sci. 27 (1987) 500–503. doi:10.1002/pen.760270704.

[43] M.J. Elwell, A.J. Ryan, H.J.M. Grunbauer, H.C. VanLieshout, An FT IR study of reaction kinetics and structure development in model flexible polyurethane foam systems, Polymer (Guildf). 37 (1996) 1353–1361. doi:10.1016/0032-3861(96)81132-3.

[44] M. Akkoyun, E. Suvaci, Effects of TiO2, ZnO, and Fe3O4 nanofillers on rheological behavior, microstructure, and reaction kinetics of rigid polyurethane foams, J. Appl. Polym. Sci. 133 (2016) 1–14. doi:10.1002/app.43658.

[45] N.S. Ramesh, S.T. Lee, Polymeric Foams: Mechanisms and Materials, First Edit, CRC Press, Boca Raton, 2004.